

Rotary Friction Welding Parameters Effects upon Mechanical Properties and Microstructure of AA2024 Weld Joints

Lakache Housseem Eddine^{a*}, May Abdelghani^a and Badji Riad^b

^aLaboratoire Génie des Matériaux, École Militaire Polytechnique, BP 17, 16042, Alger, Algeria

^bResearch Centre in industrial technologies (CRTI), B. P 64 cheraga, Algeria

ARTICLE INFO

Article history:

Received 16 August 2022

Accepted 2 February 2023

Available online

2 February 2023

Keywords:

RFW

AA2024

Mechanical behaviour

Microstructure

ABSTRACT

The present work investigates Rotary Friction Welding (RFW) of AA2024 similar joints, where the welding operations were carried out using an adapted device to a column-drilling machine (SUPEMEC J320). This work aims to determine the optimal RFW parameters from an experimental study based on mechanical tests and microscopic observations of weld joints. The best compromise, which offers the highest tensile strength value (499 MPa) corresponds to the joint obtained by using a rotational speed of 2000 rpm, a friction pressure of 12 MPa, and a forging pressure of 17 MPa. The EDX results indicate the presence of the intermetallic compounds (IMCs) in each zone of the weld joints, with varying sizes and a random distribution. This study focuses also on the microscopic analyses of the interface of weld joints and the fracture surfaces that indicates a dominant ductile fracture mode.

© 2023 Growing Science Ltd. All rights reserved.

1. Introduction

Friction welding was patented by Bevington in 1891, in which the concept of using friction heat for the welding process was applied. RFW is classified by the American Welding Society as a solid-state joining process. The RFW process is used more and more to assemble different materials such as aluminum alloys. Alves et al. (2010) tested the RFW process parameters used to have the best compromise that gives the desired tensile test results for an AA1050/AISI 304 joint, and they have shown that it is possible to obtain higher values of mechanical strength than that of AA1050; thus, they cited that the Vickers microhardness values measured in the central region, were higher than those of the Base Metal (BM). Avettand-Fènoël et al. (2016) managed to join AA2024 with pure copper by linear friction welding, a discontinuous layer of IMCs covering the interface, Al_2Cu , Al_2Cu_3 , $AlCu$, Al_4Cu_9 , and Al_3Cu_2 compounds were identified at the central zone, whereas, an out-of-equilibrium Al solid solution is detected on the AA2024 side. The growth of the IMC layer and the tensile strength of the AA5052/304 stainless steel weld joint was evaluated at various locations in the radial direction of the weld interface, the maximum tensile strength's value of 203 MPa was recorded in 0R location (Dong et al., 2020).

Recently, Li et al. (2020; 2021) studied the effect of inhomogeneous microstructure on the mechanical properties of the AA2024 RFW joints. The works done by Hu et al. (2012) aimed to understand the Friction Stir Welding (FSW) process of Al-Cu-Mg alloy tubes, to improve the tensile strength of the aluminum alloys FSW joints. Aydın et al. (2009) analyzed the FSW joints of AA2024 in various heat-treated states. They found that the maximum tensile properties and the highest hardness values were obtained for the T6 metallurgical state. Mimouni et al. (2019) report the effect of tool rotational speed on AA2017/T451 FSWed joints, their study revealed a remarkable effect of rotational speed on the mechanical behavior and microstructure of the weld joints. Etesami et al. (2015) also analyzes the influence of rotational speed on AA2014 weld joints, the results show that when the rotational speed is increased, the number of cracks and defects is dramatically reduced and the hardness is improved and it reaches a maximum value at 2000 rpm in the weld interface. The feasibility of joining by FSW

* Corresponding author. Tel.: +213 0660222376

E-mail addresses: lakache.housseem@gmail.com (L. H. Eddine)

of TiAl6V4 to AA2024-T3 and the microstructure of these joints have been studied by Dressler et al. (2009), they found that the maximum tensile strength of the joint reached 73% of the strength of BM. They highlighted microstructural changes due to welding on the aluminum side and showed that the hardness profile reveals a clear decrease at the titanium/aluminum interface.

This work aims to join AA2024 by RFW solidly and study the microstructure and mechanical properties of the weld joint that can be useful to understand the bonding nature of the RFW joint.

2. Experimental study

The pieces to weld were machined into $\text{Ø}12\text{mm}\times 50\text{mm}$, its chemical composition is indicated in **Table 1**. This study requires AA2024 rods that have undergone homogenization annealing at first, which consists of heating at 500 °C for 6h followed by cooling in the oven, which aims to erase the previous thermal and residual stresses. Next, treatment for dissolving the test pieces at 510 °C for 1h followed by quenching in frozen salty water (-40 °C), after that the samples are held for 12h at 160 °C to get the T6 metallurgical state, and finally cooled in the open air. These give the θ -phase precipitates an optimal size and distribution, this increases the strength thanks to the structural hardening phenomenon.

Table 1. Chemical composition of AA2024

Elements	Cu	Mg	Mn	Si	Fe	Zn	Al
wt.%	3.92	1.21	0.74	0.62	0.59	0.24	bal

The RFW operations were performed using a device that is fixed vertically on the table of a column-drilling machine (SUPEMEC J320) as indicated in **Fig. 1a**. The pressures are generated using a hydraulic pump and a cylinder placed in the middle of the fixing system, while the rotational movement is generated by the upper part motorized by the column-drilling machine. Combining welding tests and literature data, we have constructed a range of RFW process parameters, **Fig.1b** shows the RFW cycles adopted in this study: accosting time of 0.5 s, the contact pressure of 0.5 MPa, friction pressure of 8, 10, and 12 MPa, forging pressure of 11, 15 and 17 MPa, both friction and forging times were designed as 3 s. These parameters are used to construct five RFW cycles combined with three rotational speeds (1000, 1400, and 2000 rpm).

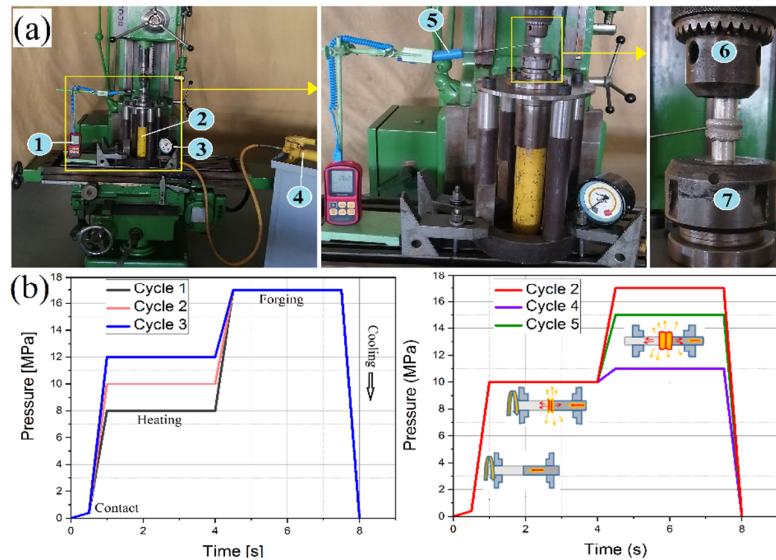


Fig. 1. (a) RFW welding setup, 1. Thermometer, 2. Hydraulic cylinder, 3. Pressure manometer, 4. Hydraulic pump, 5. K-type thermocouple, 6. Rotary side, 7. Clamping system, (b) RFW cycles

The tensile tests were performed with a constant strain rate of 10^{-3} s^{-1} using an MTS hydraulic traction machine. The tensile test specimens are prepared according to ISO 6892-1:2016(E). A load of 300 gr, and a hold time of 15 s were used to measure the Vickers microhardness across the axial direction of the weld interface. AA2024 was chemically attacked with Keller's reagent (2.5 mL $\text{HNO}_3 + 1.5\text{ mL HCl} + 1\text{ mL HF} + 95\text{ mL water}$) for 30 s and examined with an optical microscope. After tensile testing, the fracture surface morphologies were analyzed by a scanning electron microscope (SEM).

3. Results and discussion

The friction is more important in the peripheral zone than in the center because the tangential contact force is proportional to the radius. So, in the beginning, the welded bars heat on the outside, and the pasty material begins to appear in the periphery, where the temperature is higher in this zone compared to the center, after that, the temperature increases during the friction phase to favor the material flow and giving rise to a pasty toroidal flash which increases outward as shown in **Fig. 2** that

presents all welding samples. The heat propagates towards the core, gradually softening the two edges to be welded.

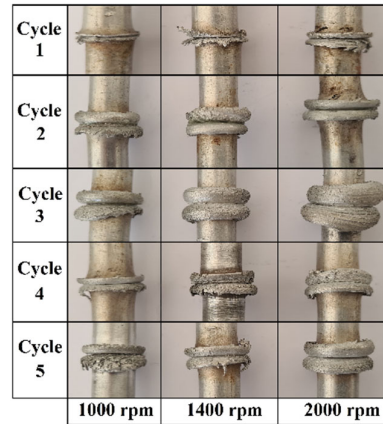


Fig. 2. Welding samples with different RFW parametres.

3.1 Microhardness profiles

The microhardness tests present results that have similar appearances and the profiles are almost symmetrical as shown in **Fig.3a-e**. Generally, there is a significant decrease in hardness values on the fixed part beyond 1 mm from the interface and spread over 3 mm, further than this interval, the hardness gradually increases.

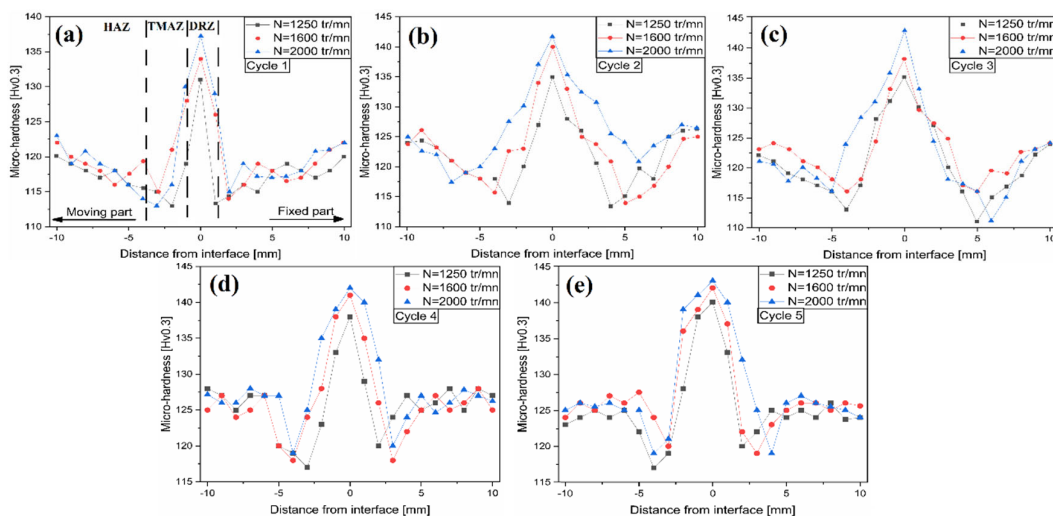


Fig. 3. Microhardness profiles combining five cycles with three rotational speeds.

Regarding the three speeds for all cycles, the readings highlight two main phases, a sudden decrease over 5 mm where the lowest hardness value is found, and a gradual increase, beyond that, the hardness values stabilize more and more. Overall, the highest hardness values were recorded for the weld joints at 2000 rpm. On the other hand, the 1250 rpm rotational speed marks the lowest hardness values, especially for cycle (1). It is observed that the highest microhardness values are obtained using cycle (5) (**Fig.3e**). This comparative study has shown that the optimum parameters are : cycle (5) and 2000 rpm, which gives the best characteristics in microhardness : 143 HV in the Dynamically Recrystallized Zone (DRZ), 138 HV in the Thermo-Mechanically Affected Zone (TMAZ), and 126 HV in the Heat-Affected Zone (HAZ). It can be seen as a region of hardness degradation, the softened region in HAZ and TMAZ that have narrow hardness values. This has the effect of weakening the joint structure. The DRZ had comparatively the greatest hardness values. The hardness measurements were strongly affected by the precipitates distribution and grain size.

3.2 Microscopic observations

Fig.4a-i shows a general view of weld joints, visible cracks can even be seen with the eyes (**Fig.4a,e** and **Fig. g**), in addition to a remarkable material flow. To eliminate cracks, it is necessary to strengthen the friction phase to give more heat to form the pasty material over the entire interface. The furthest zone from the interface is the BM, it has not undergone a temperature

rise affecting its microstructure. Defining this boundary between BM and the HAZ is often complex, it is usually characterized by a change in granulometry or the variation in hardness between the two zones.

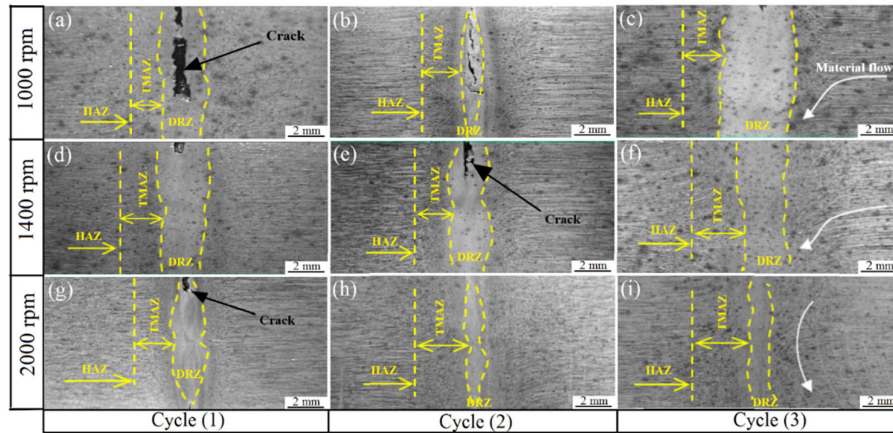


Fig. 4. Macroscopic observation of weld joints.

For the case of the weld joint using 1400 rpm and following cycle (1), the microstructure of each zone is shown in **Fig.5**. The BM is a set of very fine precipitates of different types in a monophasic solution α . Under the effect of intense plastic deformation, the DRZ's grains reorient themselves towards a circular path, their granulometry is smaller than in the other zones. The TMAZ does not undergo sufficient plastic work to recrystallize. However, there is a change in grain orientation compared to the initial direction of stretching. The HAZ only undergoes a thermal cycle resulting in the dissolution of the precipitate.

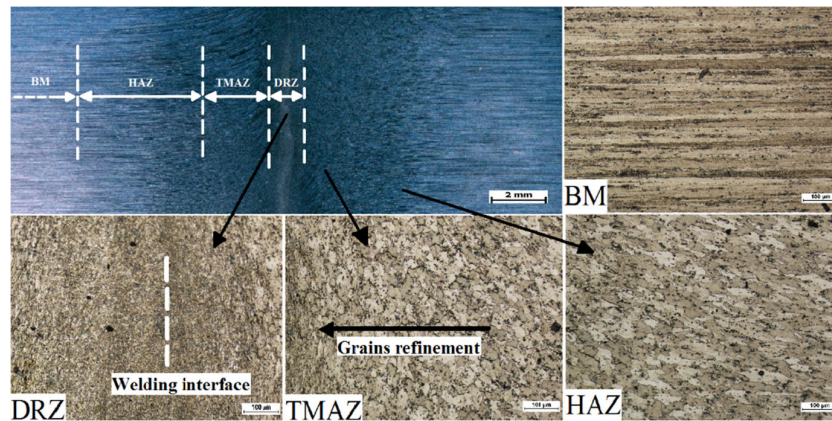


Fig. 5. Optical microstructure in different zones for cycle (1).

The heat generated during welding operation causes the phenomenon of atoms diffusion between the two welded parts, this migration holds on until the descent to room temperature. At the same time, the high mechanical stress generates severe plastic deformation, these processes are involved in the formation and migration of grain boundaries with intense disorientation, from which the grains are recrystallized, which explains the increase in microhardness in DRZ. A drop in hardness is recorded in HAZ caused by the temperature exceeding 250 °C. This temperature plays the role of a heat treatment for dissolving, which considerably reduces the size and number of precipitates and consequently a decrease in microhardness. The rotational speed and forging pressure considerably affect the microhardness of the weld joint free of macro-pores, while the frictional pressure has little influence on the joint characteristics. However, this parameter is still essential for the removal of macro-pores.

3.3 EDX analyses

The AA2000 series includes three main types of precipitates: Al-Cu, Al-Cu-Mg, and Al-Cu-Mn-Fe-Si. Generally, Al-Cu and Al-Cu-Mg IMCs correspond to Al_2Cu (θ -phase) and Al_2CuMg (S-phase) respectively. The IMCs have a diameter between 1 and a few micrometres as illustrated in Fig.6a for RFW joints corresponding to cycle (3) and 2000 rpm. To identify the existing phases in the α -matrix that is rich in Al, EDX analysis indicate their chemical composition in **Table 2**.

The grains of TMAZ undergo a significant hot deformation, which creates wavy zones in the joints and causes a change of alignment direction of the Al-Cu-Mn-Fe-Si IMCs that follow the same orientation as the grains (**Fig.6a**). The temperature and deformation reached in DRZ are maximums, leading to total dynamic recrystallization. Qualitative analysis show that some precipitates are rich in copper and others contain iron, silicon, and manganese. These IMCs are of the Al-Cu-Mn-Fe-Si type, they are numerous and located in the grains and grain boundaries.

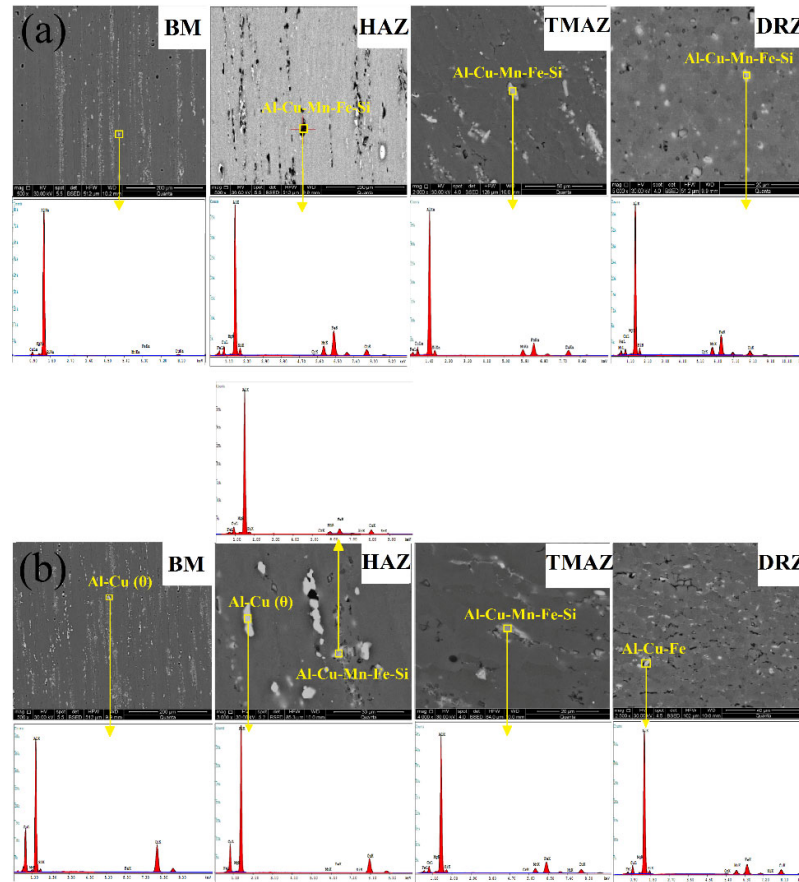


Fig. 6. SEM images and EDX spectrums of weld joint corresponding to (a) 2000 rpm and (b) 1000 rpm.

Table 2. EDX analysis

Rotational speed (rpm)	Location	Elements (wt.%)									Phase type
		Al	Cu	Mg	Ni	Fe	Mn	Si	Cr	Zn	
2000	BM	92.47	5.19	-	-	0.34	0.51	1.46	-	-	-
	HAZ	61.07	7.62	-	-	18.45	6.31	5.81	0.30	0.44	Al-Cu-Mn-Fe-Si
	TMAZ	68.42	8.69	-	-	12.30	5.09	5.49	-	-	Al-Cu-Mn-Fe-Si
	DRZ	63.85	6.50	-	-	16.81	5.85	6.27	0.24	0.47	Al-Cu-Mn-Fe-Si
1000	BM	63.40	33.09	0.70	-	0.34	-	2.46	-	-	Al-Cu(θ)
	HAZ-1	76.08	22.59	0.76	0.20	0.18	0.18	-	-	-	Al-Cu(θ)
	HAZ-2	77.15	8.69	1.47	0.14	6.15	2.39	3.68	0.15	0.18	Al-Cu-Mn-Fe-Si
	TMAZ	70.75	6.99	0.73	0.13	12.40	4.56	4.27	0.16	-	Al-Cu-Mn-Fe-Si
	DRZ	73.72	9.37	0.76	0.15	13.78	0.72	1.30	0.19	-	Al-Cu-Fe

For the rotational speed 1000 rpm, the IMCs present in BM are aligned in the direction of wire drawing with a size between 1 and 15 microns as shown in **Fig.6b**. The chemical analyses show the presence of Al-Cu precipitates. Besides, a significant porosity is also noted. In the HAZ, we can distinguish two types of precipitates, a directional cluster rich in iron (Al-Cu-Mn-Fe-Si), on the other and there is an Al-Cu phase, while a grain deformation and alignment of IMCs which belong to the Al-Cu-Mn-Fe-Si family is observed in TMAZ. There is a microcrack appearance at the grain boundaries in DRZ, this may be due to the high concentration of iron (10.78%), a particle weakening the matrix because its presence is often harmful and decreases the amount of copper participating in structural hardening. The chemical composition of the Al-Cu-Mn-Fe-Si particles presented in **Table 2** reveals the heterogeneous character of these particles, they can have different chemical formulas. The presence of all these precipitates is the origin of microhardness values fluctuations.

3.4 Tensile tests

The best tensile test results are obtained for cycle (3) as shown in **Table 3**, which offers the most remarkable value in tensile strength of 499 MPa corresponding to 2000 rpm. While the cycle (1) leads to unsatisfactory mechanical qualities. The same goes for the rest of cycles, this decrease can be explained by the relatively high welding temperature (250 °C), which caused rapidly the phenomenon of excessive aging for a relatively short duration, beyond this period, the tensile properties of the materials continue to deteriorate due to coalescence of precipitates and enlargement of their sizes, which has the effect of decreasing the joints resistance. The yield strength results show an improvement in the elastic range for most cycles, which gives a significant increase in the ductile behavior of welded metals.

Table 3. Tensile properties at different welding conditions

Cycle	Rotational speed (rpm)	Re _{0.2} (MPa)	Rm (MPa)	A (%)
1	1000	160	290	6.0
	1400	260	310	4.0
	2000	201	296	12.0
2	1000	289	338	2.5
	1400	324	387	4.0
	2000	300	456	13.0
3	1000	270	400	6.0
	1400	279	430	7.0
	2000	302	499	10.0
4	1000	276	363	3.5
	1400	204	375	6.0
	2000	270	463	12.0
5	1000	264	381	5.0
	1400	283	350	3.0
	2000	285	459	13.5

3.5 Fractographic observations

Fig.7a shows the fracture surface of a weld joint obtained by following cycle (3) and 2000 rpm. The microstructural investigation shows a very high density of cups but very low streaks, which is considered a sign of material tearing, indicating that the rupture is ductile. **Fig.7b** shows an area is taken from the fracture surface center, a very rough surface is seen corresponding to cups of different sizes. A magnification of the same area is given in **Fig. 7c** to see this morphology better, where the shape and size of these cups appear more straightforward. It can be noticed the existence of small precipitates at the bottom of some cups. Approximate measurement is made in this figure to find an average value of 15 μm for the cups radius.

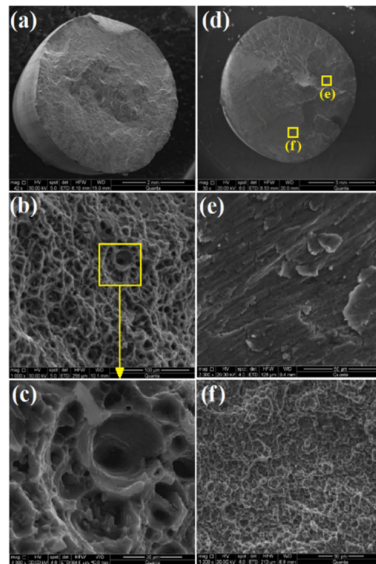


Fig. 7. (a) SEM general view of fracture surface for RFW joint using 2000 rpm, (b) and (c) Magnification of the observed morphology, (d) SEM general view of fracture surface for RFW joint using 1000 rpm, (e) and (f) Magnification of the boxed areas in (d).

Fig.7d shows a general micrograph of the fracture surface of the weld joint obtained by using cycle (1) and 1000 rpm, which indicates the existence of two different zones and the lack of adhesion in some areas of the fracture surface. In the first zone (See Fig.7e), the crack has progressed radially from several entrances, and the fracture surface seems relatively flat and smooth, and the different sliding planes are even visible. However, the AA2024 material is not hard enough to expect brittle fracture by cleavage during the early stages of cracking. Generally, the crack develops along the sliding planes of dislocations. However, the appearance of the rupture surface may suggest a pseudo-fragile rupture mode. In the second one (Fig.7f), cupular morphology occurred for most sample fracture surfaces, this rupture process generally leads to a relatively strong matting of these cups. The existence of these two zones on the fracture surface indicates that the adhesion was not complete during the RFW process for the chosen parameters.

4. Conclusion

To optimize the RFW parameters of the AA2024 joint, several variants have been adopted. An experimental study based on the analysis of microstructure and mechanical properties of the weld joints. Main conclusions can be drawn :

- (1) The highest tensile strength value (499 MPa) corresponds to the joint obtained by optimum parameters (cycle (3) and 2000 rpm).
- (2) The large microhardness values were recorded for cycle (5) and 2000 rpm, which showed values of 143, 138 and 126 HV in DRZ, TMAZ and HAZ respectively.
- (3) EDX analysis indicates the presence of IMCs with different sizes and a random distribution rather than uniform in each zone of the weld joints.
- (4) The fractographic observations of a weld joint obtained by following cycle (3) and 2000 rpm exhibit a very rough surface that indicates a ductile fracture mode.

References

- Alves, E. P., Piorino Neto, F., & An, C. Y. (2010). Welding of AA1050 aluminum with AISI 304 stainless steel by rotary friction welding process. *Journal of Aerospace Technology and Management*, 2, 301-306.
- Avettand-Fénoël, M. N., Racineux, G., Debeugny, L., & Taillard, R. (2016). Microstructural characterization and mechanical performance of an AA2024 aluminium alloy—Pure copper joint obtained by linear friction welding. *Materials & Design*, 98, 305-318.
- Aydın, H., Bayram, A., Uğuz, A., & Akay, K. S. (2009). Tensile properties of friction stir welded joints of 2024 aluminum alloys in different heat-treated-state. *Materials & Design*, 30(6), 2211-2221.
- Dong, H., Yang, J., Li, Y., Xia, Y., Hao, X., Li, P., ... & Lei, M. (2020). Evolution of interface and tensile properties in 5052 aluminum alloy/304 stainless steel rotary friction welded joint after post-weld heat treatment. *Journal of Manufacturing Processes*, 51, 142-150.
- Dressler, U., Biallas, G., & Mercado, U. A. (2009). Friction stir welding of titanium alloy TiAl6V4 to aluminium alloy AA2024-T3. *Materials Science and Engineering: A*, 526(1-2), 113-117.
- Etesami, S. A., Enayati, M. H., Karimzadeh, F., & Rasta, V. (2015). Investigating the properties of friction welded 2014 aluminum joints prepared with different rotational speeds. *Transactions of the Indian Institute of Metals*, 68(3), 479-489.
- Hu, Z. L., Yuan, S. J., Wang, X. S., Liu, G., & Liu, H. J. (2012). Microstructure and mechanical properties of Al-Cu-Mg alloy tube fabricated by friction stir welding and tube spinning. *Scripta Materialia*, 66(7), 427-430.
- Li, P., Wang, S., Dong, H., Wen, G., Yu, F., Ma, Y., & Lei, Z. (2021). Effect of inhomogeneous microstructure evolution on the mechanical properties and corrosion behavior of rotary friction welded AA2024 joints. *Materials Characterization*, 178, 111306.
- Li, P., Wang, S., Xia, Y., Hao, X., Lei, Z., & Dong, H. (2020). Inhomogeneous microstructure and mechanical properties of rotary friction welded AA2024 joints. *Journal of Materials Research and Technology*, 9(3), 5749-5760.
- Mimouni, O., Badji, R., Kouadri-David, A., Gassaa, R., Chekroun, N., & Hadji, M. (2019). Microstructure and mechanical behavior of friction-stir-welded 2017A-T451 aluminum alloy. *Transactions of the Indian Institute of Metals*, 72(7), 1853-1868.



© 2023 by the authors; licensee Growing Science, Canada. This is an open access article distributed under the terms and conditions of the Creative Commons Attribution (CC-BY) license (<http://creativecommons.org/licenses/by/4.0/>).